

Emergence and Control of Complex Behaviours in Driven Systems of Interacting Qubits with Dissipation

A. V. Andreev¹, A. G. Balanov^{2,+}, T. M. Fromhold³, M. T. Greenaway²,

A. E. Hramov¹, W. Li³, V. V. Makarov¹, A. M. Zagoskin^{2,4,*}

¹*Innopolis University, Universitetskaya Str. 1, Innopolis, 420500, Russia*

²*Department of Physics, Loughborough University, Loughborough LE11 3TU, United Kingdom*

³*School of Physics and Astronomy, University of Nottingham, Nottingham NG7 2RD, United Kingdom*

⁴*Department of Theoretical Physics and Quantum Technologies, National University of Science and Technology MISIS, 4 Leninsky Ave., Moscow 119049, Russia*

*Corresponding author: a.zagoskin@lboro.ac.uk and

⁺Corresponding author: a.balanov@lboro.ac.uk

(Dated: November 13, 2020)

Progress in the creation of large scale, artificial quantum coherent structures demands the investigation of their nonequilibrium dynamics when strong interactions, even between remote parts, are non-perturbative. Analysis of multiparticle quantum correlations in a large system in the presence of decoherence and external driving is especially topical. Still, the scaling behaviour of dynamics and related emergent phenomena are not yet well understood. We investigate how the dynamics of a driven system of several quantum elements (e.g., qubits or Rydberg atoms) changes with increasing number of elements. Surprisingly, a two-element system exhibits chaotic behaviours. For larger system sizes a highly stochastic, far from equilibrium, *hyperchaotic* regime emerges. Its complexity systematically scales with the size of the system, proportionally to the number of elements. Finally, we demonstrate that these chaotic dynamics can be efficiently controlled by a periodic driving field. The insights provided by our results indicate the possibility of a reduced description for the behaviour of a large quantum system in terms of the transitions between its qualitatively different dynamical regimes. These transitions are controlled by a relatively small number of parameters, which may prove useful in the design, characterization and control of large artificial quantum structures.

INTRODUCTION

Recent progress in experimental techniques for the fabrication, control and measurement of quantum coherent systems has allowed the routine creation of moderate-to-large arrays of controllable quantum units (e.g., superconducting qubits, trapped atoms and ions) expected to have revolutionary applications, e.g., in sensing, quantum communication and quantum computing [1–4]. They also allow the investigation of fundamental physics, such as the measurement problem [5–7], the link between the chaotic behaviour in classical systems and the corresponding dynamics in their quantum counterparts [8–12] and the relative roles of entanglement and thermalization [13–17].

The deployment of modern quantum technologies generally requires both the improvement of unit quantum elements (e.g., increasing their decoherence times) and the scaling up of quantum structures [18].

It is known that large systems comprising many functional elements tend to demonstrate emergent phenomena in their dynamics, which can not be observed in smaller systems [19, 20]. Examples include dynamical phases in driven Bose-Einstein condensates [21], synchronization in micromechanical oscillator arrays [22] and coherent THz emission from layered high-temperature superconductors [23–25]. Nevertheless, the emergent phenomena are commonly neglected when designing and investigating large-scale coherent structures. This is possi-

bly due to the absence of a convenient theoretical framework for studying these novel systems. One important open question to be tackled is how the dynamics scales with the increase of the system size (e.g., number of qubits), and what role in its change is played by emergent phenomena.

We address these questions by studying theoretically the far-from-equilibrium dynamics of a driven chain of interacting two-level quantum systems with dissipation and dephasing [Fig. 1a]. We find that even a short chain comprising between two and four elements can demonstrate chaotic behaviour. Remarkably, in systems with five or more elements a phenomenon known as hyperchaos emerges, a dynamical regime characterized by two or more positive Lyapunov exponents. Hyperchaos has features that resemble thermalisation even though the system is far from equilibrium. We show that, in contrast to thermalisation, the deterministic origin of hyperchaos allows it to be controlled either by tuning of the system parameters, or by applying an external driving force. Our results give new insights into the dynamics of large artificial quantum coherent structures, which will be important for the design and control of quantum systems such as Rydberg molecules, quantum information processors, simulators and detectors.

RESULTS

Mathematical model

Here, we investigate the dynamics of a 1D chain of N qubits driven by an external electromagnetic field in the presence of decoherence. The system under consideration is equivalent to a system of Rydberg atoms, by rescaling and reidentification of parameters [26–31]. Along with superconducting structures, Rydberg systems provide a controllable testbed for studying fundamental quantum dynamics [32–34] and for developing new quantum chemistry [35–37]. In particular, arrays of Rydberg atoms can be controlled experimentally with very high precision [38–40]. Each atom has a ground state $|g\rangle$ and an electronically excited high-energy Rydberg state $|e\rangle$ [Fig. 1b]. Rydberg states have large polarizability $\sim n^7$ (where n is the principal quantum number), which generates strong and long-range interactions between atoms [41].

To model an electromagnetically driven array of qubits (Rydberg atoms), we use the Hamiltonian

$$H = \sum_{j=1}^N \left[-\delta_\omega |e\rangle\langle e|_j + \frac{\Omega_R}{2} (|e\rangle\langle g|_j + |g\rangle\langle e|_j) \right] \quad (1)$$

$$+ \sum_{j < k} V_{i,j} |e\rangle\langle e|_j \otimes |e\rangle\langle e|_k,$$

where $\delta_\omega = \omega_l - \omega_0$ is the detuning between the laser and transition frequencies, Ω_R is the Rabi frequency (tuned by the laser field amplitude), and $V_{i,j}$ characterizes the interaction between i th and j th qubits.

The dynamics are described by the Liouville-von Neumann equation for the density matrix ρ ,

$$\dot{\rho} = -i[H, \rho] + \mathcal{L}[\rho], \quad (2)$$

where relaxation and dephasing processes are taken into account through the appropriate Lindblad operator

$$\mathcal{L}[\rho] = \gamma \sum_j \left[|g\rangle\langle e|_j \rho |e\rangle\langle g|_j - \frac{1}{2} \{ |e\rangle\langle e|_j, \rho \} \right], \quad (3)$$

with γ to be the decay rate from the excited state to the ground state. Rydberg atom interactions can range over a few tens of micrometers, larger than the physical size of the system. (The same is true for superconducting qubits interacting through a resonator field mode). Therefore, to simplify the analysis, we can initially assume that interactions are identical for any pair of qubits, $V_{i,j} = V$ [see Fig. 1a,b]. For a system of N qubits, ρ has the dimensionality of its Hilbert space, 2^N .

This problem can be greatly simplified by substituting a fully factorized density matrix approximation, $\rho \approx \prod_j \otimes \rho_j$, in (2). Here ρ_j is the (one-particle) density matrix of the j th qubit. This approximation is justified for a

partially quantum coherent system, for which it has been shown accurately to describe experimental measurements on qubits, up to the corrections due to two-point correlations [38, 42–45]. In such a case, the quantum coherence between spatially separated elements is disrupted, e.g. by local ambient noise [46].

Rewriting the factorized density matrix ρ in terms of the population inversion of the j th qubit, $w_j = (\rho_j)_{11} - (\rho_j)_{00}$, and its coherence, $q_j = (\rho_j)_{10} = (\rho_j)_{01}^*$, yields:

$$\dot{w}_j = -2\Omega \Im q_j - (w_j + 1);$$

$$\dot{q}_j = i \left[\Delta - c \sum_{k \neq j} (w_k + 1) \right] q_j - \frac{1}{2} q_j + i \frac{\Omega}{2} w_j. \quad (4)$$

In (4) the dimensionless time $\tau = \gamma t$ (i.e. $\dot{x} \equiv dx/d\tau = \gamma^{-1} dx/dt$), $\Omega = \Omega_R/\gamma$, $\Delta = \delta_\omega/\gamma$, and $c = Va/\gamma$, where a is the lattice constant. In more detail the derivation of (4) is discussed in Section A in Supplementary Materials.

Emergence of chaos and hyperchaos

Here we study the dynamical regimes of chains of interacting qubits. To characterise the complexity (randomness) of the emergent chaos and hyperchaos we calculate the full spectrum of the Lyapunov exponents [47].

First we analyze two coupled qubits ($N = 2$). Previously, it has been shown that interplay between the energy pumping and dissipation can eventually trigger self-sustained state population oscillations in this system and even lead to the emergence of bistability, when homogeneous and antiferromagnetic states coexist [27]. Our investigation reveals another interesting phenomenon associated with deterministic chaos, which emerges via a cascade of period-doubling bifurcations for a periodic oscillations [47]. In Fig. 1c, we show a color map illustrating the dependence of the largest Lyapunov exponent Λ_1 on Δ and Ω . A transition from yellow to black reflects the change from smaller to larger values of Λ_1 . The diagram clearly demonstrates the presence of chaotic dynamics, for which $\Lambda_1 > 0$, in considerable areas of the parameter plane shaded by black color. This shows that the discovered chaos is a robust phenomenon existing in our system over wide parameter ranges. Notably, for certain parameter values it coexists with the antiferromagnetic steady state. The detailed descriptions of the bifurcation transitions and analysis of the Lyapunov exponents that characterize the stability of long-term dynamics are presented in Section B in Supplementary Materials.

For $N = 3$ and 4, the same type of chaotic dynamics exists in the system. However, surprisingly, for $N \geq 5$ a new type of chaotic dynamics appears, whose stability is characterized by more than one positive Lyapunov exponent. This type of chaos is known as *hyperchaos* [48]. A map of different dynamical regimes in the (Δ, Ω) parameter plane is shown in Fig. 2a for $N = 5$ and $c =$

5. This diagram was built by calculating the spectrum of Lyapunov exponents for the various limit sets that exist in the (Δ, Ω) -plane. When all the Lyapunov exponents are negative, there is a stable equilibrium state (white in the diagram). If the largest Lyapunov exponent equals 0 the oscillations are periodic (cyan). If the largest two Lyapunov exponents are both 0, the dynamics are quasiperiodic (red). However, when one or two Lyapunov exponents are positive, there is chaos (green) or hyperchaos (black), respectively.

Figure 2b illustrates the bifurcation transitions between the different dynamical regimes when $\Omega = 2.5$ and Δ changes along the yellow dashed line in Fig. 2a. The blue curves represent the evolution of the four largest Lyapunov exponents $\Lambda_1 > \Lambda_2 > \Lambda_3 > \Lambda_4$. A number of distinctive phases emerge as we increase Δ from 1 to 9. The stable equilibrium state, which exists for small Δ , switches to a periodic solution as a result of an Andronov-Hopf bifurcation at $\Delta \approx 1.7$, where Λ_1 becomes zero. At $\Delta \approx 3.55$ the periodic oscillations lose their stability via a Neimark-Sacker bifurcation, resulting in the onset of quasiperiodic oscillations ($\Lambda_1 = \Lambda_2 = 0$). Increasing Δ further leads to chaotic dynamics.

To better illustrate the transition to the chaotic regime, in Fig. 2c we present a zoom of the region of Fig. 2b framed by the black rectangle. The corresponding bifurcation diagram, shown in Fig. 2d, is constructed by plotting the points corresponding to the local maxima $w_{1,max}$ in the time evolution of $w_1(t)$, calculated for given Δ . For a particular value of Δ , periodic solutions are represented by one or few single dots on the graph, while the complex sets of many points for a specific Δ reflect quasiperiodic or chaotic dynamics. As Δ increases, the quasiperiodic oscillations where $\Lambda_1 = \Lambda_2 = 0$ [Fig. 2c] are replaced (at $\Delta \approx 3.732$) by complex periodic oscillations due to saddle-node bifurcation. These periodic oscillations are characterized by $\Lambda_1 = 0$ and $\Lambda_{2,3} < 0$ [Fig. 2c] and represented in Fig. 2d by few isolated dots for a fixed Δ . For $\Delta \gtrsim 3.744$, the periodic solutions undergo a cascade of period-doubling bifurcations giving rise to chaos with one positive Lyapunov exponent at $\Delta \approx 3.75$ [Fig. 2c]. The period-doubling bifurcations do not affect the spectrum of Lyapunov exponents of the stable solution, since the latter remains periodic. However, each period-doubling causes additional Lyapunov exponent to approach zero [Fig. 2c], which manifests itself via doubling of the number of dots in Fig. 2d. Thus for $N = 5$, the bifurcation mechanism leading to the onset of chaos stays the same as for the case of $N=2$. Further investigation shows that this mechanism is also present at larger N .

Increasing Δ makes the chaotic oscillations more complicated and leads to the gradual development of hyperchaos, which emerges at $\Delta \approx 4.4$ [see Fig. 2b]. This transition is linked to further instability of already unstable periodic orbits, which form the skeleton of the chaotic

attractor. Accumulation of the corresponding bifurcations causes the second Lyapunov exponent to become positive.

We find that period-doubling is the most common, but not the only, route to chaos exhibited by the system. Figure 2a reveals some direct transitions from the red region where the dynamics is quasiperiodic to the green region where the dynamics are chaotic. This behaviour can indicate the mechanism of torus destruction for the transition to chaos. However, we did not specifically investigate the effect of this particular mechanism on the development of hyperchaos.

The dynamics of $N = 5$ coupled qubits in different dynamical regimes is exemplified in Fig. 3. Typical periodic solution is presented in Fig. 3a. Here, $n = 1, \dots, 5$ denotes the qubit number in the chain, t is time, and the color scale indicates the value of w_n . All qubits oscillate with the same frequency, but with different phases. However, the phase shift is constant for each pair of qubits, meaning that they are synchronized. The latter is also indicated by the clearly periodic pattern in Fig. 3a. The quasiperiodic regime when $\Delta = 3.73$ is shown in Fig. 3b. Now the phase shifts between oscillations of different qubits are no longer constant, and the periodic pattern of the spatio-temporal dynamics is lost, reflecting the loss of synchronization.

Chaotic oscillations for $\Delta = 4.05$ are illustrated in Fig. 3c. Here, the qubit chain demonstrates erratic behavior, which is in marked contrast to the ordered dynamics presented in Figs. 3a and b. Figure 3d shows typical hyperchaotic oscillations calculated for $\Delta \approx 4.95$. In this regime, the oscillations in the chain become even more complicated than the chaotic behavior in Fig. 3c, and now demonstrate no specific time-scales in $w_n(t)$. The hyperchaotic behavior persists up to $\Delta \approx 8.0$, after which it rapidly switches to chaotic and then periodic solutions. For $\Delta > 8.53$, all oscillations disappear, and all long-term solutions in the system correspond to stable equilibrium.

In order to further examine the presence of the multistability in the dynamics of the chain, we return to the evolution of the Lyapunov exponents as Δ changes from 9 down to 1. Values of $\Lambda_{1,2,3,4}$ for this case are shown red in Fig. 2b. The plot shows that the stable homogeneous steady state ($\Lambda_1 = \Lambda_2 = \Lambda_3 = \Lambda_4 < 0$) exists down to $\Delta \approx 5.491$, where it suddenly changes to hyperchaotic oscillations. Thus, within the interval of Δ between 5.491 and 9.0 the homogeneous fixed point co-exists with different inhomogeneous regimes including other types of equilibria, periodic and quasiperiodic oscillations, chaos and hyperchaos [blue graphs in Fig. 2b]. Multistability therefore appears to be a generic phenomenon, existing in chains of different size.

Analysis of chains with $N > 5$ reveals that hyperchaos is not only preserved in the system, but becomes more complicated as more Lyapunov exponents become positive. The results of our analysis are summarized in Fig.

4, where the number of positive Lyapunov exponents, M , is shown as a function of the number of qubits in the chain. The graph shows an almost linear growth, at a rate suggesting that adding two or three qubits leads to the appearance of an additional positive Lyapunov exponent. This phenomenon originates from a weak correlation between the oscillations in distant qubits. As a result, the addition of a subsystem, comprising two or more qubits is able to demonstrate chaotic dynamics and adds one more positive value to the spectrum of the Lyapunov exponents. Since, for a given coupling, the smallest chaotic subsystem comprises two qubits, their inclusion produces one more positive Lyapunov exponent. The number of Lyapunov exponents grows roughly proportionally to the number N of qubits rather than with the dimensionality 2^N of the Hilbert space of the system. This indicates the possibility of a reduced description of its dynamics. In such a case the transitions between qualitatively different, distinct dynamical regimes are controlled by a relatively small number of independent dimensionless parameters.

For large N , multiple positive Lyapunov exponents make the oscillations very complicated, demonstrating broadband continuous spectra, which are similar to random fluctuations in solids [49, 50]. In addition, we found out that these hyperchaotic phenomena are preserved for non-identical qubits and open chains, as well as in chains with more complex qubit-coupling topology than those discussed above. The spatial correlations, the spectra of the chain oscillations calculated for different numbers of qubits, and Lyapunov analysis of chains with non-identical qubits and more complex topology are discussed in Sections C and D in Supplementary Materials.

To study the significance of the system's dimensionality, we analyze 2D $L \times L$ lattices of L^2 interacting qubits (Fig. 5a). As for 1D rings, these square lattices exhibit chaotic (for 2×2 lattices) and hyperchaotic behavior (for 3×3 and larger lattices). Figure 5c illustrates the Lyapunov exponents spectrum for a 3×3 square lattice. We observe two areas ($2.7 < \Delta < 3.8$ and $\Delta \approx 5.8$) of chaos, one small area of hyperchaos with two positive Lyapunov exponents ($\Delta \approx 4.2$), and two areas of hyperchaos with three positive exponents ($4.4 < \Delta < 5.3$ and $6.05 < \Delta < 7.6$). Therefore for a lattice of 9 qubits we observe a complicated behavior with three positive Lyapunov exponents, which is similar behavior to that we observe for a ring of 9 qubits. We investigate lattices with several values of L of nodes and find almost linear growth of the number of positive Lyapunov exponents with increasing the number of qubits in the lattice (see Fig. 5b). We can conclude that emergence of hyperchaos does not depend on the dimensionality of the system.

Chaos control via a coherent driving field

This dynamical complexity has a deterministic origin, which could be controlled (suppressed or enhanced) by an applied external field. Previously, it was demonstrated that a periodic perturbation can suppress hyperchaos with two positive Lyapunov exponents [51, 52]. Here, we apply a periodic modulation to the laser field amplitude which modulates the Rabi frequency:

$$\Omega = \Omega_m [1 + M \sin(2\pi ft)]. \quad (5)$$

where Ω_m is the amplitude of the Rabi frequency, whilst M and f are the modulation index and the frequency of modulation, respectively. We consider the case when $N = 15$, a large but practically feasible number of qubits such that the system shows hyperchaos, characterized by four positive Lyapunov exponents and a broadband spectrum. Figure 6 presents the eleven largest conditional Lyapunov exponents (a) and the corresponding bifurcation digram (b) calculated for $\Omega_m = 2.5$, $c = 5$, $\Delta = 5.0$, $M = 0.684$ and f changing from 0 to 1.8.

Due to the periodic modulation, chaos is suppressed in certain parameter regions. For f between 0.7 and 0.8 we find complex periodic oscillations characterized by the largest Lyapunov exponent less than 0 [see Fig. 6a] and multiple branches in the bifurcation diagram [Fig. 6b]. Within the interval $f \in (0.9, 1.1)$ we find period-one oscillations (one maxima per period) and Lyapunov exponents $\ll 0$, corresponding to highly stable regular oscillations in this regime. In addition, the same controlling signal is able to significantly increase the complexity of hyperchaotic oscillations and a corresponding increase in the value of the largest Lyapunov exponent. For example, when $f \approx 0.3$ the largest Lyapunov exponent becomes almost three time larger than in the case without the application of the signal ($f = 0$). Otherwise the number of positive Lyapunov exponents can be increased by 1 ($f = 1.2$) or 2 ($f = 1.4$). Our results demonstrate that periodic modulation of laser field amplitude can be used as an efficient method to control very complex hyperchaos in qubit arrays.

DISCUSSION

We have shown that the interplay between dissipation and energy pumping in quantum systems comprising chains of qubits can produce highly nontrivial emergent phenomena associated with the onset of complex chaotic and hyperchaotic oscillations even in the absence of multi-particle entanglement. The complexity of the hyperchaos increases with the number of elements in the chain. The number of positive Lyapunov exponents grows linearly with the number of qubits, that is, as only log of the dimensionality of the Hilbert space. This indicates the possibility of a reduced description of the

quantum system by a small (in comparison to the dimensionality of the Hilbert space) number of dimensionless parameters. This observation is consistent with the fact that the manifold of all quantum states that can be generated by arbitrary time-dependent local Hamiltonians in a polynomial time occupies an exponentially small volume in the Hilbert space of the system [53].

Our results demonstrate a mechanism for randomizing the evolution of coupled qubits, which arises due to dynamical phenomena far from equilibrium and is thus unrelated to thermalization processes despite the superficial similarity. The model we have used is generic and can be applied and implemented directly in, e.g., chains of qubits or electromagnetically driven superconducting qubits. Our results will be important for the development of large quantum systems, where multi-point entanglement is neither required nor supported [42, 43, 54]. In particular, they suggest a controllable way of switching between different dynamical regimes via regular to chaos transitions either by tuning the parameters of the system or by applying a controlling signal via modulation of laser field amplitude, as another approach towards controlling quantum state dynamics [55]. Our results are of interest for the development of quantum random number generators [56] and quantum chaotic cryptography [57, 58]. A natural extension of this research will consider the effect of interqubit entanglement on the complexity revealed here, and whether it can be utilised for controlling this far-from-equilibrium behavior.

Another interesting task will be to study how quantum signatures of classical chaos such as the growth rate of out-of-time-ordered correlators [59] behave in the presence of hyperchaos. Preliminary results on the integration of the original quantum model (2), briefly discussed in Section E in Supplementary Materials, indicate that the complexity of chain dynamics depends highly non-trivially on the parameters of the Hamiltonian (1). However, a detailed analysis of the dynamical regimes and their characteristics in the presence of entanglement, and especially of the question about the universality of these regimes and parameters that control them, requires extensive further research, which we hope this paper will stimulate.

METHODS

Lyapunov exponents calculation

The Lyapunov exponents were calculated for the stable limit sets, which correspond to the solutions of the model equations as time $t \rightarrow \infty$. Since we apply the periodic modulation (5) to the system (4), the Lyapunov exponents we calculate in this case are called conditional and missing one zero exponent, unlike the common Lyapunov exponents spectrum [60]. To determine them, we imple-

ment $3N$ perturbations vectors, where N is the number of units in the system, and use periodic Gram-Schmidt orthonormalization of the Lyapunov vectors to avoid a misalignment of all the vectors along the direction of maximal expansion [61, 62].

Bifurcation diagrams

In order to construct a bifurcation diagram we plot the points corresponding to the local maxima $w_{1,max}$ in the time-evolution of $w_1(t)$, calculated for given Δ and Ω .

DATA AVAILABILITY STATEMENT

The data that support the findings of this study are available from the corresponding authors upon reasonable request.

CODE AVAILABILITY STATEMENT

All code used in the paper are available from the corresponding authors upon reasonable request.

ACKNOWLEDGEMENTS

A.M.Z. and A.G.B. thank Prof. S. Watabe for illuminating discussions. This work was supported in part by EPSRC (grant EP/M006581/1), the grant from the Ministry of Science and Higher Education of the Russian Federation in the framework of Increase Competitiveness Program of NUST MISiS, Grant No. K2-2020-001 and Russian Foundation for Basic Research (RFBR) 18-32-20135. W.L. acknowledges support from the UKIERI-UGC Thematic Partnership No. IND/CONT/G/16-17/73, EPSRC Grant No. EP/R04340X/1, and support from the University of Nottingham.

AUTHOR CONTRIBUTIONS

A.M.Z., A.G.B. and A.E.H. conceived, designed and supervised the project. The theoretical calculations were performed by A.M.Z. (analytical) and A.V.A., V.V.M., A.E.H. and A.G.B. (numerical). A.G.B., T.M.F., M.T.G., W.L. and A.M.Z. wrote the manuscript. All authors discussed the results and contributed to the manuscript.

COMPETING INTERESTS

The authors declare no competing interests.

-
- [1] Walport, M. & Knight, P. The quantum age: technological opportunities (2016).
- [2] Georgescu, I. & Nori, F. Quantum technologies: an old new story. *Physics World* **25**, 16 (2012).
- [3] Knight, P. & Walmsley, I. UK national quantum technology programme. *Quantum Science and Technology* **4**, 040502 (2019).
- [4] Acín, A. *et al.* The quantum technologies roadmap: a European community view. *New Journal of Physics* **20**, 080201 (2018).
- [5] Zurek, W. H. Decoherence, einselection, and the quantum origins of the classical. *Reviews of Modern Physics* **75**, 715 (2003).
- [6] Zurek, W. H. Quantum darwinism. *Nature Physics* **5**, 181–188 (2009).
- [7] Xiong, H.-N., Lo, P.-Y., Zhang, W.-M., Nori, F. *et al.* Non-markovian complexity in the quantum-to-classical transition. *Scientific Reports* **5**, 13353 (2015).
- [8] Lambert, N., Chen, Y.-n., Johansson, R. & Nori, F. Quantum chaos and critical behavior on a chip. *Physical Review B* **80**, 165308 (2009).
- [9] Aßmann, M., Thewes, J., Fröhlich, D. & Bayer, M. Quantum chaos and breaking of all anti-unitary symmetries in Rydberg excitons. *Nature Materials* **15**, 741–745 (2016).
- [10] Fiderer, L. J. & Braun, D. Quantum metrology with quantum-chaotic sensors. *Nature Communications* **9**, 1–9 (2018).
- [11] Gao, T. *et al.* Observation of non-Hermitian degeneracies in a chaotic exciton-polariton billiard. *Nature* **526**, 554–558 (2015).
- [12] Zhu, G.-L. *et al.* Single-photon-triggered quantum chaos. *Physical Review A* **100**, 023825 (2019).
- [13] Chaudhury, S., Smith, A., Anderson, B., Ghose, S. & Jessen, P. S. Quantum signatures of chaos in a kicked top. *Nature* **461**, 768–771 (2009).
- [14] Zhang, W., Sun, C. & Nori, F. Equivalence condition for the canonical and microcanonical ensembles in coupled spin systems. *Physical Review E* **82**, 041127 (2010).
- [15] Neill, C. *et al.* Ergodic dynamics and thermalization in an isolated quantum system. *Nature Physics* **12**, 1037–1041 (2016).
- [16] Turner, C. J., Michailidis, A. A., Abanin, D. A., Serbyn, M. & Papić, Z. Weak ergodicity breaking from quantum many-body scars. *Nature Physics* **14**, 745–749 (2018).
- [17] Lewis-Swan, R., Safavi-Naini, A., Bollinger, J. J. & Rey, A. M. Unifying scrambling, thermalization and entanglement through measurement of fidelity out-of-time-order correlators in the dicke model. *Nature Communications* **10**, 1–9 (2019).
- [18] Dowling, J. P. & Milburn, G. J. Quantum technology: the second quantum revolution. *Philosophical Transactions of the Royal Society of London. Series A: Mathematical, Physical and Engineering Sciences* **361**, 1655–1674 (2003).
- [19] Hegel, G. W. F. *The Science of Logic* (Cambridge University Press, 2015).
- [20] Engels, F. *Anti-Dühring Herr Eugen Dühring's revolution in science* (Progress Publishers, 1969).
- [21] Piazza, F. & Ritsch, H. Self-ordered limit cycles, chaos, and phase slippage with a superfluid inside an optical resonator. *Physical Review Letters* **115**, 163601 (2015).
- [22] Zhang, M., Shah, S., Cardenas, J. & Lipson, M. Synchronization and phase noise reduction in micromechanical oscillator arrays coupled through light. *Physical Review Letters* **115**, 163902 (2015).
- [23] Ozyuzer, L. *et al.* Emission of coherent THz radiation from superconductors. *Science* **318**, 1291–1293 (2007).
- [24] Savel'ev, S., Yampol'skii, V., Rakhmanov, A. & Nori, F. Terahertz Josephson plasma waves in layered superconductors: spectrum, generation, nonlinear and quantum phenomena. *Reports on Progress in Physics* **73**, 026501 (2010).
- [25] Welp, U., Kadowaki, K. & Kleiner, R. Superconducting emitters of THz radiation. *Nature Photonics* **7**, 702–710 (2013).
- [26] Weimer, H., Müller, M., Lesanovsky, I., Zoller, P. & Büchler, H. P. A Rydberg quantum simulator. *Nature Physics* **6**, 382–388 (2010).
- [27] Lee, T. E., Häffner, H. & Cross, M. Antiferromagnetic phase transition in a nonequilibrium lattice of Rydberg atoms. *Physical Review A* **84**, 031402 (2011).
- [28] Lee, T. E., Haefner, H. & Cross, M. Collective quantum jumps of Rydberg atoms. *Physical Review Letters* **108**, 023602 (2012).
- [29] Ostrovskaya, E. A. & Nori, F. Giant Rydberg excitons: Probing quantum chaos. *Nature materials* **15**, 702–703 (2016).
- [30] Labuhn, H. *et al.* Tunable two-dimensional arrays of single Rydberg atoms for realizing quantum Ising models. *Nature* **534**, 667–670 (2016).
- [31] Minganti, F., Miranowicz, A., Chhajlany, R. W. & Nori, F. Quantum exceptional points of non-Hermitian Hamiltonians and Liouvillians: The effects of quantum jumps. *Physical Review A* **100**, 062131 (2019).
- [32] Bendkowsky, V. *et al.* Observation of ultralong-range Rydberg molecules. *Nature* **458**, 1005–1008 (2009).
- [33] Löw, R. Rydberg atoms: two to tango. *Nature Physics* **10**, 901–902 (2014).
- [34] Basak, S., Chougale, Y. & Nath, R. Periodically driven array of single Rydberg atoms. *Physical Review Letters* **120**, 123204 (2018).
- [35] Butscher, B. *et al.* Atom–molecule coherence for ultralong-range Rydberg dimers. *Nature Physics* **6**, 970–974 (2010).
- [36] Niederprüm, T. *et al.* Observation of pendular butterfly Rydberg molecules. *Nature Communications* **7**, 1–6 (2016).
- [37] Eiles, M. T., Tong, Z. & Greene, C. H. Theoretical prediction of the creation and observation of a ghost trilobite chemical bond. *Physical Review Letters* **121**, 113203 (2018).
- [38] Zeiher, J. *et al.* Coherent many-body spin dynamics in a long-range interacting Ising chain. *Physical Review X* **7**, 041063 (2017).
- [39] Labuhn, H. *et al.* Tunable two-dimensional arrays of single Rydberg atoms for realizing quantum Ising models. *Nature* **534**, 667–670 (2016).
- [40] Barredo, D. *et al.* Coherent excitation transfer in a spin chain of three Rydberg atoms. *Physical Review Letters* **114**, 113002 (2015).
- [41] Saffman, M., Walker, T. G. & Mølmer, K. Quantum information with Rydberg atoms. *Reviews of Modern Physics* **82**, 2313 (2010).
- [42] Zagoskin, A., Rakhmanov, A., Savel'ev, S. & Nori, F. Quantum metamaterials: Electromagnetic waves in

- josephson qubit lines. *physica status solidi (b)* **246**, 955–960 (2009).
- [43] Macha, P. *et al.* Implementation of a quantum metamaterial using superconducting qubits. *Nature Communications* **5**, 1–6 (2014).
- [44] Gaul, C. *et al.* Resonant Rydberg dressing of alkaline-earth atoms via electromagnetically induced transparency. *Physical Review Letters* **116**, 243001 (2016).
- [45] Zeiher, J. *et al.* Many-body interferometry of a Rydberg-dressed spin lattice. *Nature Physics* **12**, 1095–1099 (2016).
- [46] Aolita, L., De Melo, F. & Davidovich, L. Open-system dynamics of entanglement: a key issues review. *Reports on Progress in Physics* **78**, 042001 (2015).
- [47] Anishchenko, V. S. *Dynamical Chaos, Models and Experiments: Appearance Routes and Structure of Chaos in Simple Dynamical Systems* (World Scientific Publishing, Singapore, 1995).
- [48] Rössler, O. An equation for hyperchaos. *Physics Letters A* **71**, 155–157 (1979).
- [49] Field, S., Venturi, N. & Nori, F. Marginal stability and chaos in coupled faults modeled by nonlinear circuits. *Physical Review Letters* **74**, 74 (1995).
- [50] Kogan, S. *Electronic noise and fluctuations in solids* (Cambridge University Press, 2008).
- [51] Xiao-Hui, Z. & Ke, S. The control action of the periodic perturbation on a hyperchaotic system. *Acta Physica Sinica (Overseas Edition)* **8**, 651 (1999).
- [52] Sun, K., Liu, X., Zhu, C. & Sprott, J. Hyperchaos and hyperchaos control of the sinusoidally forced simplified Lorenz system. *Nonlinear Dynamics* **69**, 1383–1391 (2012).
- [53] Poulin, D., Qarry, A., Somma, R. & Verstraete, F. Quantum simulation of time-dependent Hamiltonians and the convenient illusion of Hilbert space. *Physical Review Letters* **106**, 170501 (2011).
- [54] Fitzpatrick, M., Sundaresan, N. M., Li, A. C., Koch, J. & Houck, A. A. Observation of a dissipative phase transition in a one-dimensional circuit qed lattice. *Physical Review X* **7**, 011016 (2017).
- [55] Zhang, J., Liu, Y.-x., Wu, R.-B., Jacobs, K. & Nori, F. Quantum feedback: theory, experiments, and applications. *Physics Reports* **679**, 1–60 (2017).
- [56] Herrero-Collantes, M. & Garcia-Escartin, J. C. Quantum random number generators. *Reviews of Modern Physics* **89**, 015004 (2017).
- [57] Monifi, F. *et al.* Optomechanically induced stochastic resonance and chaos transfer between optical fields. *Nature Photonics* **10**, 399–405 (2016).
- [58] de Oliveira, G. & Ramos, R. V. Quantum-chaotic cryptography. *Quantum Information Processing* **17**, 40 (2018).
- [59] Chávez-Carlos, J. *et al.* Quantum and classical Lyapunov exponents in atom-field interaction systems. *Physical Review Letters* **122**, 024101 (2019).
- [60] Pyragas, K. Conditional Lyapunov exponents from time series. *Physical Review E* **56**, 5183 (1997).
- [61] Oseledets, V. I. A multiplicative ergodic theorem. Characteristic Ljapunov, exponents of dynamical systems. *Trans. Moscow Math. Soc.* **19**, 197–231 (1968).
- [62] Wolf, A., Swift, J. B., Swinney, H. L. & Vastano, J. A. Determining Lyapunov exponents from a time series. *Physica D: Nonlinear Phenomena* **16**, 285–317 (1985).

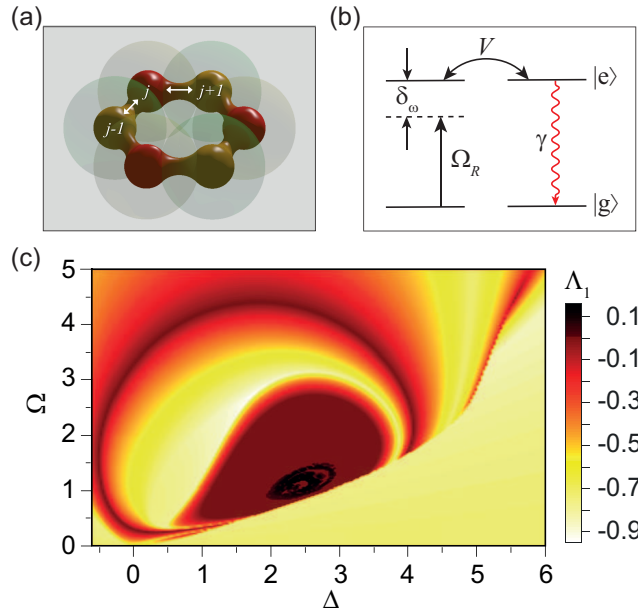


FIG. 1: **Schematic representation of interacting qubits and the largest Lyapunov exponent dependence on model parameters for the case of two qubits.** **a** Schematic representation of a circular chain of six interacting quantum units (e.g., Rydberg atoms or qubits), labelled by integer indexes and coupled via nearest neighbor interaction. **b** Atomic-level configuration reflected in the model [Eqs. (1-3)]. Coherent laser excitation from the ground state $|g\rangle$ to an excited (“Rydberg”) state $|e\rangle$ with a Rabi frequency Ω_R and detuning δ_ω , incoherent spontaneous decay γ , and the Rydberg interaction when an excited qubit shifts the transition frequency of a neighboring qubit by V . **c** Dependence of the largest Lyapunov exponent Λ_1 on Δ and Ω calculated for $c = 5$ for the system of 2 coupled qubits. The color scale intensity indicates the value of Λ_1 .

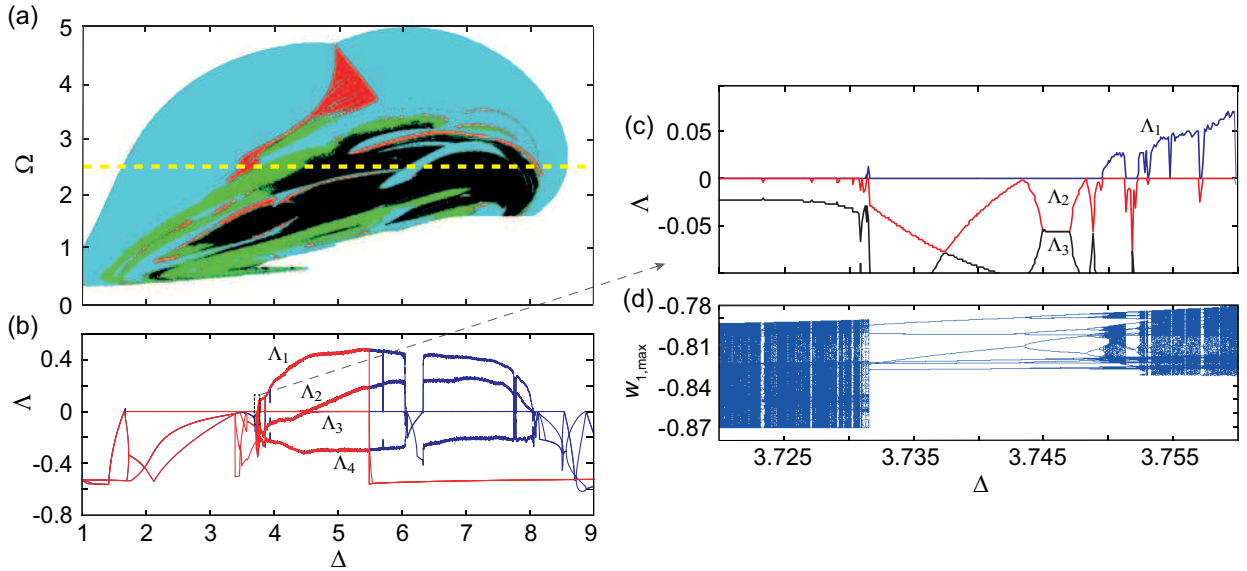


FIG. 2: **Hyperchaos in a ring of five qubits.** **a** Map showing areas of (Δ, Ω) space corresponding to different regimes of long-term behavior for a ring of five qubits. Black denotes areas of hyperchaos with two positive Lyapunov exponents, green is a region of chaos with one positive Lyapunov exponent, cyan is a periodic regime, red areas correspond to quasiperiodic behavior, white is a steady state regime. **b** Variation of the four largest Lyapunov exponents with Δ ; blue dots correspond to Δ increasing from 1 to 9, red dots – to Δ decreasing down to 1. **c** A zoom of the region of **b** within the black rectangle. **d** Single-parametric bifurcation diagram corresponding to **c**, in which the vertical positions of each point correspond to the local maxima of $w_1(t)$. For all figures $\Omega = 2.5$.

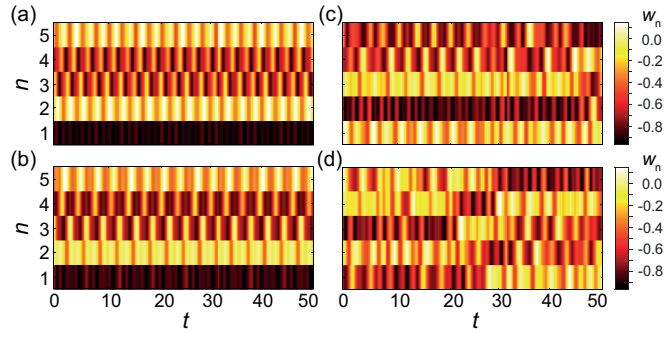


FIG. 3: **Time evolution of w_n for 5 qubits.** **a** Periodic [$\Delta = 3.74$], **b** quasiperiodic [$\Delta = 3.73$], **c** chaotic [$\Delta = 4.05$] and **d** hyperchaotic [$\Delta = 4.95$] oscillations; n labels an qubit in the chain.

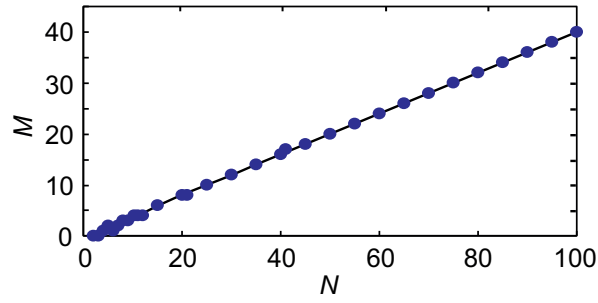


FIG. 4: **Number of positive Lyapunov exponents M vs. number of qubits N in the ring chain.** $\Delta = 5$, $\Omega = 2.5$, $c = 5$.

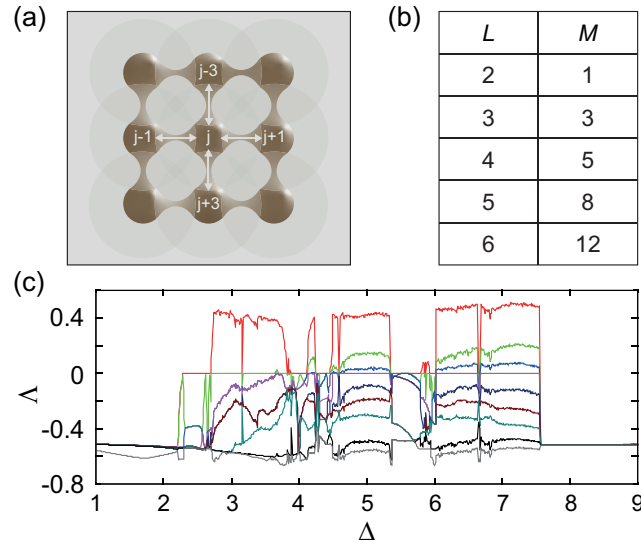


FIG. 5: **2D $L \times L$ lattices of L^2 interacting qubits.** **a** Schematic representation of a square lattice of nine interacting quantum units (e.g., Rydberg atoms or qubits), labelled by integer indexes and coupled via nearest neighbor interaction. **b** Number of positive Lyapunov exponents M vs. lattice size L in the $L \times L$ lattice calculated for $\Delta = 5$, $\Omega = 2.0$, $c = 5$. **c** Variation of the eight largest Lyapunov exponents with Δ for a square lattice of 9 qubits, $\Omega = 2.0$.

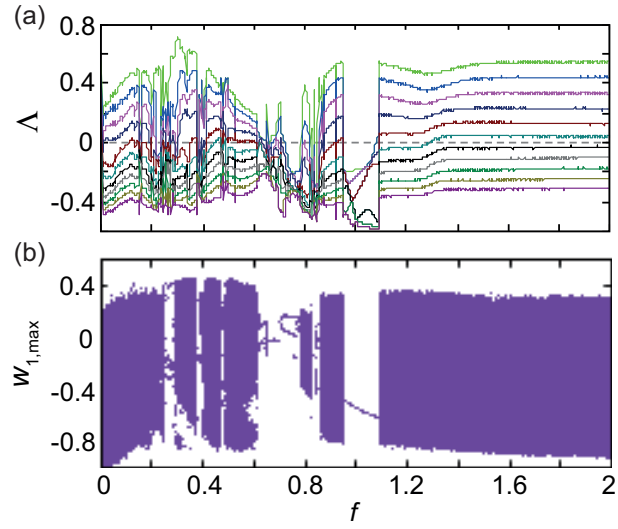


FIG. 6: **Chaos control.** **a** Conditional Lyapunov exponents spectrum and **b** bifurcation diagram for a ring of 15 qubits by means of an external parametric effect for $\Omega_m = 2.5$, $c = 5$, $\Delta = 5.0$, $M = 0.684$.

Emergence and Control of Complex Behaviours in Driven Systems of Interacting Qubits with Dissipation.

SUPPLEMENTARY MATERIALS.

A. V. Andreev¹, A. G. Balanov^{2,+}, T. M. Fromhold³, M. T. Greenaway²,

A. E. Hramov¹, W. Li³, V. V. Makarov¹, A. M. Zagoskin^{2,4,*}

¹*Innopolis University, Universitetskaya Str. 1, Innopolis, 420500, Russia*

²*Department of Physics, Loughborough University, Loughborough LE11 3TU, United Kingdom*

³*School of Physics and Astronomy, University of Nottingham, Nottingham NG7 2RD, United Kingdom*

⁴*Department of Theoretical Physics and Quantum Technologies,*

National University of Science and Technology MISIS, 4 Leninsky Ave., Moscow 119049, Russia

*Corresponding author: a.zagoskin@lboro.ac.uk and

+Corresponding author: a.balanov@lboro.ac.uk

A. Model of electromagnetically driven interacting qubits with decoherence and dissipation

The standard description of a set of interacting qubits is provided by the Ising Hamiltonian,

$$H = \sum_j H_j + \sum_{j < k} U_{jk}, \quad (1)$$

with

$$H_j = -\frac{1}{2} [\epsilon_j \sigma_j^z + \delta_j \sigma_j^x], \quad U_{jk} = J_{jk} \sigma_j^z \sigma_k^z. \quad (2)$$

Here the Pauli operators, σ_j^α , describe the transitions between qubit states, ϵ_j and δ_j are, respectively, the bias and the tunneling matrix element in the j th qubit, and J_{jk} is the qubit-qubit coupling. In the case of superconducting qubits of various kinds all these parameters can, in principle, be tuned in experiments (see, e.g., [1, 2]). Moreover, since certain degree of control is possible for all types of currently available qubits, including Rydberg atom-based, the model (1,2) is generic. Expressing the Pauli matrices in terms of projectors to the ground and excited states of the qubits, $|g\rangle, |e\rangle$,

$$\begin{aligned} \sigma_j^z &\equiv |g\rangle\langle g|_j - |e\rangle\langle e|_j \equiv \hat{1}_j - 2|e\rangle\langle e|_j; \\ \sigma_j^x &\equiv |e\rangle\langle g|_j + |g\rangle\langle e|_j; \hat{1}_j \equiv |g\rangle\langle g|_j + |e\rangle\langle e|_j, \end{aligned} \quad (3)$$

we can rewrite (2) as

$$\begin{aligned} H_j &= -\frac{1}{2} \epsilon_j \hat{1}_j + \epsilon_j |e\rangle\langle e|_j - \frac{1}{2} \delta_j [|e\rangle\langle g|_j + |g\rangle\langle e|_j], \\ U_{jk} &= J_{jk} [\hat{1}_j - 2|e\rangle\langle e|_j] \otimes [\hat{1}_k - 2|e\rangle\langle e|_k]. \end{aligned} \quad (4)$$

This yields the Hamiltonian (1) in the form

$$\begin{aligned} H &= \sum_j \left\{ \left[\epsilon_j - 2 \sum_k J_{jk} \right] |e\rangle\langle e|_j - \frac{1}{2} \delta_j [|e\rangle\langle g|_j + |g\rangle\langle e|_j] \right\} \\ &\quad + 4 \sum_{jk} J_{jk} |e\rangle\langle e|_j \otimes |e\rangle\langle e|_k + \left[-\frac{1}{2} \sum_j \epsilon_j + \sum_{jk} J_{jk} \right]. \end{aligned}$$

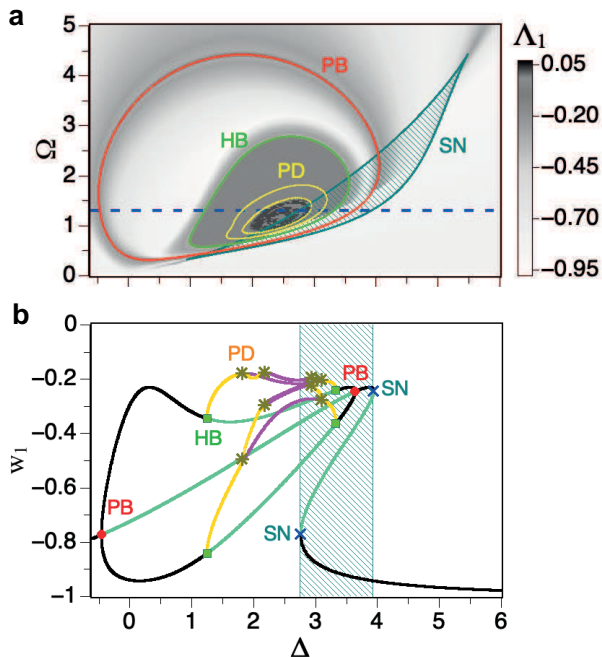
Up to the irrelevant total energy shift, $\Delta E = \left[-\frac{1}{2} \sum_j \epsilon_j + \sum_{jk} J_{jk} \right]$, and parameter relabeling, this Hamiltonian is an inhomogeneous version of the interaction-representation Hamiltonian of a system of Rydberg atoms in a laser field [3, 4]. In the mapping of (4) on Eq.(1), δ_ω corresponds to $(\epsilon_j - 2 \sum_k J_{jk})$, i.e., the role of detuning is played by the negative of the mean-field excitation energy of a qubit. The role of the Rabi frequency is, quite naturally, taken over by (the negative of) the matrix element of interlevel transition, $-\delta_j$. The interqubit couplings J_{jk} map to the factor $V/8(N-1)$ in Eq.(1). As mentioned above, for the exact analogy with Rydberg atoms we must assume that there is no dispersion of qubit properties, but such an assumption is not necessary when investigating the qubit dynamics.

The evolution for one-qubit density matrix ρ_j is obtained directly from the von Neumann equation,

$$\frac{d}{dt} \prod_j \rho_j = \frac{1}{i} [H, \prod_j \rho_j] + \mathcal{L}[\prod_j \rho_j],$$

by tracing out all qubits except the j th one. In terms of Pauli matrices (denoting the unit matrix by σ_0) and a one-qubit density matrix is expressed through the population inversion and coherence as $\rho_j = (1/2)(\sigma_j^0 - w_j \sigma_j^z + 2\Re q_j \sigma_j^x + 2\Im q_j \sigma_j^y)$. Therefore tracing out $(N-1)$ qubits with $k \neq j$ leaves in the von Neumann equation only terms linear in $\dot{w}_j, \dot{q}_j, w_j, q_j$, plus a nonlinear term originating from the interqubit zz -coupling in Eq.(2). This term produces an effective mean-field correction to detuning. Gathering the coefficients at $\sigma_j^{x,y,z}$, we obtain Eqs.(4) in the main text.

The dynamics of the system described by Eqs. (4) in the main text was first studied in [3] for the case of Rydberg atoms with laser driving and spontaneous emission. The authors of that work investigated the transition between the uniform and antiferromagnetic phases induced by variation of the controlling parameters of the system. In particular, they discovered the existence of a novel oscillatory phase and bistability between the uniform and antiferromagnetic phases. Here we focus on the detailed

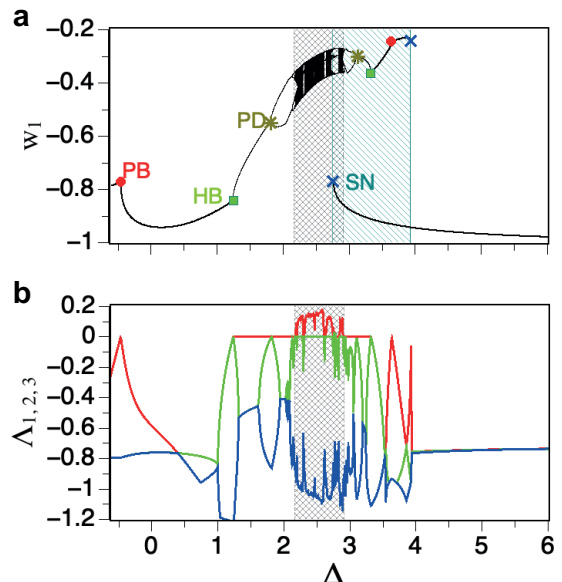


SUPPLEMENTARY FIGURE 1: (Color online) **a** Two-parametric bifurcation diagram calculated for $c = 5$. Red curve (PB), green curve (HB), yellow curves (PD) and dark-green curve (SN) are loci of pitch-fork, Andronov-Hopf, period-doubling and saddle-node bifurcations, respectively. The gray scale intensity indicates the value of the largest Lyapunov exponent Λ_1 . **b** Single-parametric bifurcation diagram along the blue dashed line in **a** for $\Omega = 1.3$. Black and green points correspond to stable and unstable fixed points, respectively; brown/magenta points indicate the maximal value of w_1 corresponding to stable/unstable periodic oscillations. The red circles (PB), green squares (HB), dark-yellow asterisks (PD) and blue crosses (SN) denote pitchfork, Hopf, period-doubling and saddle-node bifurcation, respectively. In both **a** and **b** the cross-hatched area marks the region of multistability, where a homogeneous fixed point coexists with other solutions.

bifurcation analysis of multiple coupled qubits systems and on the transitions to the chaotic dynamics found in our investigation.

B. Dynamics of two qubits

The results of our analysis for two qubits are summarized in Suppl. Fig. 1a, where the bifurcation diagram in the parameter plane (Δ, Ω) is presented for the coupling parameter $c = 5$ defined in Eqs. (4) in the main text. The red line labeled PB indicates the pitchfork bifurcation, which is associated with the appearance/disappearance of two stable symmetric fixed points (steady states). The green (HB) line corresponds to the onset of the Hopf bifurcation, where stable periodic oscil-



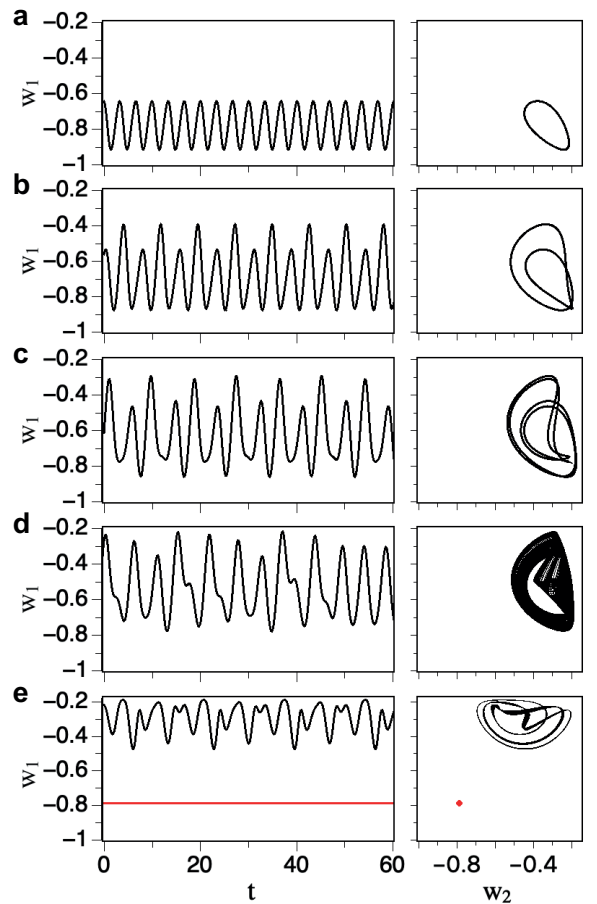
SUPPLEMENTARY FIGURE 2: (Color online) Single-parametric bifurcation diagram illustrating evolution of stable regimes with variation of Δ . The black dots correspond to the Poincaré section $\dot{w}_1 + \dot{w}_2 = 0$. **b** Dependence of the three largest Lyapunov exponents $\Lambda_{1,2,3}$ on Δ . Both **a** and **b** were calculated for $c = 5$ and $\Omega = 1.3$, along the blue dashed line in Suppl. Fig. 1a. The shaded area in **a** marks the region of multistability, cross-hatched areas [in both **a** and **b**] denote the chaos region.

lations emerge/vanish in the system. The yellow curves (PD) mark the position of period-doubling bifurcations of the periodic oscillations. The dark-cyan curve (SN) shows the locus of saddle-node bifurcation, which gives birth to a pair of stable and saddle fixed points. This curve encompasses the cross-hatched area of the parameter plane, where the homogeneous fixed point, for which $w_1 = w_2$ and $q_1 = q_2$, coexists with other equilibrium or oscillatory solutions. The bifurcation lines are superimposed on a grayscale map illustrating the dependence of the largest Lyapunov exponent Λ_1 on Δ and Ω . The Lyapunov exponents were calculated for the stable limit sets, which correspond to the solutions of the model equations as time $t \rightarrow \infty$. To determine them, we utilized the theory and numerical approaches discussed in [5, 6]. The negative values of Λ_1 correspond to the fixed points (equilibrium states), zero values mean the periodic or quasiperiodic solutions, while positive Λ_1 evidences the presence of deterministic chaos [7]. A transition from white to black in Suppl. Fig. 1a reflects the change from smaller to larger values of Λ_1 . The diagram clearly demonstrates the existence of chaotic dynamics ($\Lambda_1 > 0$) in considerable areas of the parameter plane shaded by dark-gray/black colors.

To better illustrate the bifurcation transitions, in

Suppl. Fig. 1b we present a single-parametric bifurcation diagram calculated for $\Omega = 1.3$, i.e. along the blue dashed horizontal line in Suppl. Fig. 1a. Each point on the diagram corresponds to the maximal value of the variable w_1 calculated for a given Δ . The black and green colors denote stable and unstable fixed points, respectively, while brown and magenta points correspond to stable and unstable periodic solutions. With Δ increasing from a negative value, the homogeneous fixed point undergoes a pitchfork bifurcation at $\Delta \approx -0.465$ (red circle labeled as PB). As a result, it becomes unstable, and in its vicinity a pair of symmetric inhomogeneous fixed points is born. Notably, it was shown in [3] that this bifurcation corresponds to phase transition between the uniform and antiferromagnetic phases. With further increase of Δ , each of these inhomogeneous (antiferromagnetic) fixed points loses its stability via the Hopf bifurcation at $\Delta \approx 1.238$ (green square HB), which leads to the appearance of stable periodic oscillations (yellow points). In turn, these oscillations become unstable due to another period-doubling bifurcation at $\Delta \approx 1.819$ (dark-yellow asterisk PD) giving birth to a stable periodic solution with doubled period. With varying Δ , these period-two oscillations undergo another period-doubling bifurcation at $\Delta \approx 2.136$ leading to the emergence of stable period-four oscillations. This sequence of period-doubling bifurcations continues with the growth of Δ , producing an infinite set of unstable periodic solutions with different periods. Eventually, this cascade of bifurcations leads to the appearance of chaotic oscillations, which are characterized by $\Lambda_1 > 0$, at $\Delta \approx 2.17$. If Δ grows even further, the bifurcation scenario discussed above develops in the opposite direction. Namely, chaos disappears through the inverse cascade of period-doubling bifurcations that starts at $\Delta \approx 2.90$. This is followed by a Hopf bifurcation ($\Delta \approx 3.322$), where the oscillations cease, and then inverse pitch-fork bifurcation ($\Delta \approx 3.636$), where symmetric ferromagnetic fixed points merge and annihilate, while the homogeneous fixed point becomes stable. The homogenous fixed points are involved in a pair of saddle-node bifurcations (blue crosses SN) at $\Delta \approx 2.756$ and $\Delta \approx 3.931$. This creates folds on the bifurcation diagram, which suggests hysteresis and forms a region of bistability (shaded area), where a homogeneous fixed point (black dots in the lower part of the diagram) coexists with other solutions (black or brown points in the upper part of the diagram).

Supplementary Figure 2a demonstrates how the stable solutions of the model equations evolve with varying Δ . The diagram exhibits the points of a Poincaré section of phase trajectories calculated for a range of Δ . We have chosen the Poincaré section defined by the equation $\dot{w}_1 + \dot{w}_2 = 0$ as it produces a diagram convenient for interpretation. Thus, for a given Δ , a single point in the bifurcation diagram represents either a fixed point or periodic oscillations of w_1 . Similarly, several separated points cor-



SUPPLEMENTARY FIGURE 3: Time evolution of w_1 (left panels) and the (w_1, w_2) projection of the phase trajectories of the stable regimes calculated for $\Omega = 1.3$, $c = 5$ and **a** $\Delta = 1.5$, **b** $\Delta = 1.939$, **c** $\Delta = 2.147$, **d** $\Delta = 2.5$ and **e** $\Delta = 2.76$.

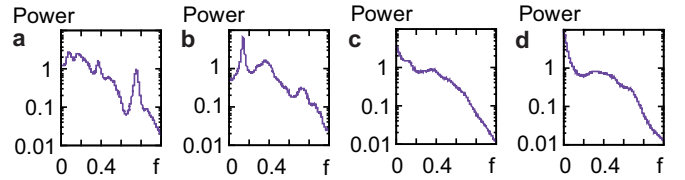
respond to period-added oscillations and a complex set of points reflects chaotic behavior. The bifurcation points PB, HB, PD and SN have the same interpretations as in Suppl. Fig. 1b. Since the branches of inhomogeneous solutions are symmetric with respect to swapping the state variables $\{\omega_1, q_1 \Leftrightarrow \omega_2, q_2\}$, for simplicity, Suppl. Fig. 2a shows only one branch of inhomogeneous solutions.

For comparison, Suppl. Fig. 2b shows the three largest Lyapunov exponents, $\Lambda_1 > \Lambda_2 > \Lambda_3$, calculated for the same range of Δ as in Suppl. Fig. 2a. One can see that in the vicinity of every bifurcation point, one of the Lyapunov exponents approaches zero thus signaling the development of instability. For small values of Δ , before the point HB, all the Lyapunov exponents are negative, which indicates that the stable regime is a steady state (fixed point). Above HB, the “period-one” stable oscillations appear in the system, which are represented in Suppl. Fig. 2a by a single point for each value of Δ . An example of such oscillations for $\Delta = 1.5$ is shown in Suppl. Fig. 3a. The left panel shows the time-domain

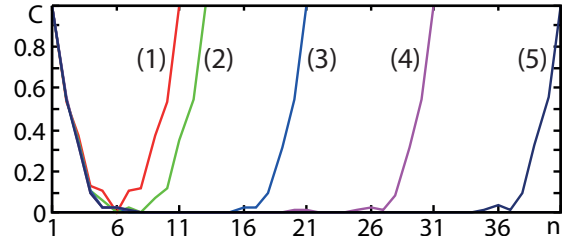
realization of w_1 , while the right panel depicts the projection of the phase trajectories of the oscillations on the (w_2, w_1) plane. The phase trajectories correspond to a limit cycle, seen as a single-loop closed curve. Period-doubling bifurcation PD destabilises period-one oscillations and gives birth to stable period-two oscillations, an example of which is shown in Suppl. Fig. 3b for $\Delta = 1.939$. The time-domain realization of this regime (left panel) shows two maxima per period, which in phase space implies a two-loop limit cycle (right panel). In Suppl. Fig. 2b the period-two limit cycle is represented by two points for each given Δ . After the second period-doubling bifurcation, the period-two oscillations lose their stability producing period-four oscillations. These oscillations are represented in Suppl. Fig. 2a by four points for a given Δ . The oscillations have four maxima per period [Suppl. Fig. 3c] and their phase trajectory forms a four-loop limit cycle. All periodic regimes are characterized by one zero Lyapunov exponent, whilst all other Lyapunov exponent are negative [see Suppl. Fig. 2b].

The evolution of period-added limit cycles with the variation of Δ leads to the appearance of deterministic chaos, whose areas of existence are cross-hatched in Figs. 2a,b. In Suppl. Fig. 2a the chaos is mapped as a complex set of points. A typical chaotic time evolution is shown in the left panel of Suppl. Fig. 3d. Although the oscillations superficially demonstrate a certain order, they are irregular, unstable, do not have any distinct period, and their phase trajectories never close; although from time to time they return to the same area of the phase space [right panel of Fig 3d]. These oscillations are characterized by one positive and one zero Lyapunov exponent, with all other Lyapunov exponents being negative. This sequence of Lyapunov exponents evidences the chaotic character of the oscillations [7]. One can see that the chaos region in Suppl. Fig. 2a is interspersed with “windows of periodicity”, where the chaos is replaced by complex periodic solutions. In Suppl. Fig. 2b these windows are reflected by Λ_1 falling back to zero. The emergence of these windows of periodicity is typical for chaos born through a cascade of period-doubling bifurcations [7].

The range of Δ corresponding to bistability in the system is shown in Suppl. Fig. 2a as the cross-hatched area limited by a pair of SN points. Within this range, the homogeneous fixed point (the lower branch of the bifurcation diagram) coexists with different inhomogeneous solutions (the upper branch of the diagram). It is noteworthy that, depending on the value of Δ , the latter solution can be either another fixed point or periodic oscillations, or even chaos. An example of the coexistence of a homogeneous fixed point and chaos is shown in Suppl. Fig. 3e. The chaos in this example is weaker than that in Suppl. Fig. 3d because Λ_1 is smaller in the former. This is also reflected in the behavior of the oscillations. For instance, the phase trajectories in Suppl. Fig. 3d, forming



SUPPLEMENTARY FIGURE 4: Power-frequency (f) spectrum of $w_1(t)$ calculated for the dynamics of qubit chains consisting of 4 **a**, 8 **b**, 10 **c**, 20 **d** qubits for $\Omega = 2.5$, $c = 5$, $\Delta = 5.0$.



SUPPLEMENTARY FIGURE 5: Correlation coefficient, C , of the first qubit in the chain calculated versus the index, n , of the other qubit for chains with $N = 10$ (line 1), 12 (line 2), 20 (line 3), 30 (line 4) and 40 (line 5), and for $\Omega = 2.5$, $c = 5$, $\Delta = 5.0$.

a multi-band chaotic attractor, look more regular than the dynamics in Suppl. Fig. 3e, where the chaotic attractor demonstrates a single band with very irregular orbits.

C. Spectra of hyperchaotic oscillations

Figure 4 presents the power spectrum for chaotic and hyperchaotic oscillations, which emerge in the ring chains of qubits with varying N for fixed $\Omega = 2.5$, $c = 5$ and $\Delta = 5.0$. For $N = 4$ (a) the system demonstrates chaotic oscillations, which are characterized by one positive Lyapunov exponent. The chaotic oscillations demonstrate a broadband continuous spectrum with a distinct peak near the frequency $f = 0.8$ corresponding to the characteristic time scale of the oscillations. For $N = 8$ [Suppl. Fig. 4b], the oscillations existing for the parameters above become hyperchaotic with three positive Lyapunov exponents. In the Fourier spectrum, the position of the characteristic peak shifts towards lower frequency $f \approx 0.11$, which reflects the change of the character of the chaotic behavior. In addition, the peak itself becomes less pronounced as its height considerably decreases compared to the background. As N further increases (c), the distinctive characteristic peaked power spectrum disappears, and for $N > 12$ (d) the spectrum of hyperchaos varies smoothly with f , demonstrating a shape that is typical of random noise in solids, e.g. hot-electron noise in semiconductors [8].

To shed light on the dependence of the number of the positive Lyapunov exponents, M , versus N , presented in Suppl. Fig. 5, we calculated the linear correlation coefficients $c_{m,n}$, characterizing the correlations between the oscillations of the m^{th} and n^{th} qubits in the chain

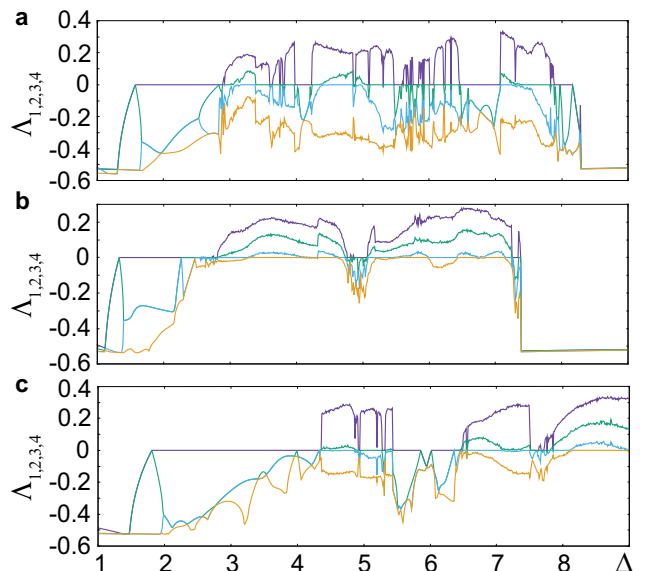
$$c_{m,n} = \frac{\langle (w_m(t) - \langle w_m \rangle)(w_n(t) - \langle w_n \rangle) \rangle}{\sqrt{\langle (w_m(t) - \langle w_m \rangle)^2 \rangle \langle (w_n(t) - \langle w_n \rangle)^2 \rangle}}, \quad (5)$$

where $\langle \cdot \rangle$ is the time average, and $m, n = 1, \dots, N$. The n dependence of the coefficient $C = c_{1,n}$ calculated for different N is shown in Suppl. Fig. 5. Each curve is symmetric with maxima $C = 1$ for $n = 1$ and $n = N + 1$ reflecting the fact that we consider ring chains, where the first and $(N + 1)$ th qubits coincide. For all N , the correlation C drops to almost zero for $n = 6$. Thus, the oscillation of the first qubit is practically unaffected by the dynamics of the 6th one. Due to this drop of correlation in chains with $N > 6$, the inclusion of a chaotic oscillator into the chain simply adds a new positive Lyapunov exponent to the spectrum. Previously, we have shown that chaotic dynamics can emerge as a cooperative phenomenon when at least two qubits interact with each other. Such interactions could provide a qualitative explanation for the almost linear dependence of M on N shown in Suppl. Fig. 5, where the inclusion of every 2-3 extra qubits into the chain with $N > 6$ produces an additional positive Lyapunov exponent for the given values of the parameters.

D. Non-identical qubits

We examined the existence of chaos and hyperchaos in chains of non-identical qubits with nearest neighbor interactions, both in ring formation and open chains, and also in a ring chain where each qubit connects with two neighbors on each side. The parameters of each qubit were detuned with a random mismatch of up to 10% of their average values: $\Delta_i = \Delta + \delta\Delta_i$, $\Omega_i = \Omega + \delta\Omega_i$, and $c_i = c + \delta c_i$. Figure 6 presents the variation of the four largest Lyapunov exponents with Δ for (a) five non-identical qubits in the ring chain, (b) ten non-identical qubits in an open chain, and (c) ten non-identical qubits in a ring chain, where each qubit interacts with two neighbors on each side. All graphs are plotted for $\Omega = 2.5$ and $c = 5$. The parameters' mismatch for the graphs in Suppl. Fig. 6a (Suppl. Fig. 6 b,c) are summarized in Suppl. Tab. I (II) respectively.

The graphs in Suppl. Fig. 6 reveal the areas of Δ that correspond to one or few positive Lyapunov exponents, i.e. areas of existence of chaos and hyperchaos, in all types of the chains considered. The latter confirms the generic character of chaos and hyperchaos phenomena in various chains of coherent quantum systems.



SUPPLEMENTARY FIGURE 6: Variation of the four largest Lyapunov exponents with Δ calculated for **a** five non-identical qubits in a ring chain with the parameters given in Supplementary Table I; **b** ten non-identical qubits in non-ring chain; **c** ten non-identical qubits, each connected to two nearest neighbors on each side. The parameters for **b** and **c** are summarized in Supplementary Table II; for all graphs $\Omega = 2.5$, $c = 5$.

i	$\delta\Omega_i$	$\delta\Delta_i$	δc_i
1	-0.2	+0.45	-0.1
2	-0.15	0	+0.45
3	+0.05	-0.4	0
4	0	-0.05	+0.4
5	+0.2	+0.25	-0.35

SUPPLEMENTARY TABLE I: Parameters of the five individual qubits used to calculate the graphs in Suppl. Fig. 6a, where index i labels the qubit position in the chain.

E. Entangled qubits.

To obtain insights into the role of entanglement on the dynamics of a qubit chain, we numerically integrate the von Neumann equation (Eq.(2) in the main text) for the N -particle density matrix, without any simplifying assumptions. To illustrate the results, we consider a chain of $N = 5$ qubits with nearest-neighbor interaction and calculate the average Rydberg population $\langle E \rangle(t) = \sum_j \text{Tr} |e\rangle \langle e|_j / N$, where Tr denotes the trace of the density matrix. Supplementary Figure 7 shows the typical time dependence of $\langle E \rangle(t)$ calculated for fixed values of $\Delta = 2.5$, $V = 5$, $\gamma = 0.01$ and various Ω . For small $\Omega = 0.3$, the expectation value $\langle E \rangle$ demonstrates coherent, almost harmonic, oscillations (a). As Ω grows, the system transitions through quasiperiodic (b), noise-like (c), and, finally, re-entrant quasiperiodic

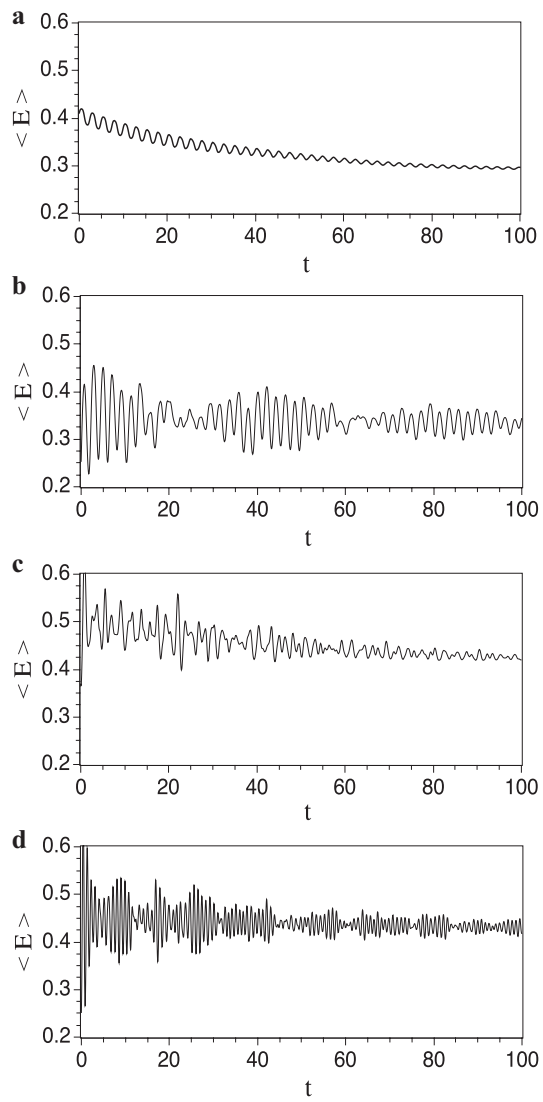
i	$\delta\Omega_i$	$\delta\Delta_i$	δc_i
1	-0.25	+0.45	-0.4
2	+0.1	0	+0.15
3	-0.15	-0.3	0
4	0	-0.1	+0.4
5	+0.2	+0.25	-0.2
6	-0.35	+0.35	-0.5
7	+0.05	-0.2	+0.25
8	-0.05	-0.35	+0.1
9	+0.15	+0.05	+0.45
10	+0.25	+0.5	-0.25

SUPPLEMENTARY TABLE II: Parameters of the ten individual qubits used to calculate the graphs in Suppl. Fig. 6b,c, where index i labels the qubit position in the chain.

decaying oscillations (d). A detailed analysis of this result, as well as investigation of the transition from the fully entangled to the factorized case in the presence of entanglement-disrupting processes, will be presented in a separate paper.

- sity Press, 2011).
- [2] Gu, X., Kockum, A. F., Miranowicz, A., Liu, Y.-x. & Nori, F. Microwave photonics with superconducting quantum circuits. *Physics Reports* **718**, 1–102 (2017).
- [3] Lee, T. E., Häffner, H. & Cross, M. Antiferromagnetic phase transition in a nonequilibrium lattice of Rydberg atoms. *Physical Review A* **84**, 031402 (2011).
- [4] Lee, T. E., Häffner, H. & Cross, M. Collective quantum jumps of Rydberg atoms. *Physical Review Letters* **108**, 023602 (2012).
- [5] Oseledets, V. I. A multiplicative ergodic theorem. Characteristic Ljapunov exponents of dynamical systems. *Trans. Moscow Math. Soc.* **19**, 197–231 (1968).
- [6] Wolf, A., Swift, J. B., Swinney, H. L. & Vastano, J. A. Determining Lyapunov exponents from a time series. *Physica D: Nonlinear Phenomena* **16**, 285–317 (1985).
- [7] Anishchenko, V. S. *Dynamical Chaos, Models and Experiments: Appearance Routes and Structure of Chaos in Simple Dynamical Systems* (World Scientific Publishing, Singapore, 1995).
- [8] Kogan, S. *Electronic noise and fluctuations in solids* (Cambridge University Press, 2008).

[1] Zagoskin, A. M. *Quantum engineering: theory and design of quantum coherent structures* (Cambridge Univer-



SUPPLEMENTARY FIGURE 7: Time evolution of $\langle E \rangle$ calculated for $\Delta = 2.5$, $V = 5$, $\gamma = 0.01$ and **a** $\Omega = 0.3$, **b** $\Omega = 1.3$, **c** $\Omega = 3.3$ and **d** $\Omega = 5.7$.